Crystal chemistry and physical-chemical behaviour of RE-E-bearing phosphates and arsenates

The case study of Mt. Cervandone

Francesco Pagliaro
Dipartimento di Scienze della Terra "A. Desio", Università degli Studi di Milano, via Botticelli 26, Milano, Italia
DOI:10.19276/plinius.2023.01.009

INTRODUCTION

Rare Earth Elements

Rare Earth Elements (REE) correspond to the lanthanoid group, Sc and Y, which are recognized as indisputably fundamental materials for several economic sectors, mostly connected with high-tech industry and the so-called "green" energy. Within the last few decades, their market has experienced a strong increase. The applications of REE are bound to several modern technologies, like, but not limited to, permanent magnets, battery alloys, catalysts for petroleum and automotive sectors, glass additives, polishing and phosphors in monitors (e.g., Blengini et al., 2020).

Rare Earth Elements are conventionally split into two major groups, the Light REE (LREE) and Heavy REE (HREE), based on their atomic radii and electronic configuration of the 4*f* electron shell: LREE comprising the Ce-Gd group, while the HREE includes the Tb-Lu series; in addition, Y was included as one of the HREE, being its atomic radius intermediate between those of Ho and Er, while Sc is not included in any of the two groups, although it is worth to mention that the smaller ionic radius of Sc makes it to behave as one of the HREE.

Mt. Cervandone

The present study focuses on several mineral samples from hydrothermal quartz fissures outcropping at the Mt Cervandone (Lepontine Alps), in Piemonte, Italy. From the geographical point of view, the area of interest is in the Verbano-Cusio-Ossola province, within the natural park "Parco dell'Alpe Veglia e dell'Alpe Devero. From the geological perspective, the Cervandone area is located within the Penninic domain of the Central Alps and, more specifically, within the Lower Penninic units.

The Mt. Cervandone is one of the most renowned REE deposits of the Alps, known among both collectors and scientists for its unusual and changing nature of the REE- and As-bearing mineralogical species. Unfortunately, despite the huge number of studies focused on the Mt. Cervandone area, most of them relate to the mineralogy of unusual specimens and very little efforts have been dedicated to unveil its geological features. Indeed, there are only few studies (Guastoni et al., 2006; Guastoni et al., 2013) concerning the REE-source in Mt. Cervandone. It is known that the origin of REE-minerals is connected to the NYF pegmatites: within the pegmatites, the RE-E-bearing minerals are rather abundant, and the pegmatites likely represent the pristine REE source (Graeser & Roggiani 1976) with allanite-(Ce) representing the most likely source mineral (Alessandro Guastoni, personal communication). On the other side, within the quartz fissures, the occurrence of REE-bearing minerals is rather sporadic (Guastoni et al., 2006).

Allanites can undergo a complete dissolution, leaving centimetric allanite-shaped voids, often filled by monazite-(Ce) and synchyste-(Ce) (Alessandro Guastoni, personal communication). The decomposition of allanites leads to a REE enrichment in the hydrothermal fluids, which determined the crystallization of REE-minerals within the quartz fissures.

ATO_4 minerals

Among the several REE-minerals belonging to the alpine-fissures of the Cervandone complex, in the context of the present project, two arsenates [chernovite-(Y) and gasparite-(Ce)] and two phosphates [xenotime-(Y) and monazite-(Ce)] have been selected. All of them belong to the so-called ATO_4 group. The expression ATO_4 is a general term used in the literature to define ternary, inorganic compounds, usually oxides. Within ATO_4, *A* and *T* represent two cations, not necessarily different, that can combine with oxygen (and seldom with other anions) in several structural topologies, including, but not limited to, scheelite, zircon, monazite, fergusonite, barite, quartz, cristobalite, wolframite and rutile topologies (Fukunga & Yamaoka, 1979).

In the current project, the charge and rather large size assumed by the *A*-cation (i.e., REE^{3+}, in this particular case) also restrict the chemical composition (and charge) of the possible *T*-site, which is limited to As, P, V, Cr and

Si. Thus, within the ATO_4 minerals object of the present study, *A* stands for REE, Ca, U and Th, whereas *T* stands for tetrahedrally-coordinated cations (As, P, V, as well as minor Si and Cr). Concerning the structural topologies, almost exclusive attention is dedicated to the zircon and monazite structures, shown by the four minerals object of this work: chernovite-(Y) [nominally $YAsO_4$], xenotime-(Y) [nominally YPO_4], gasparite-(Ce) [nominally $CeAsO_4$] and monazite-(Ce) [nominally $CePO_4$]. Chernovite-(Y) and xenotime-(Y) are characterized by a zircon-type structure; monazite-(Ce) and gasparite-(Ce) share the same monazite-type topology. The crystal structure of these minerals has been the object of a large number of studies and reviews (*e.g.*, Clavier et al., 2011; Finch & Hanchar, 2003).

The zircon-type topology is characterized by a highly symmetric tetragonal *I*-centered lattice (space group $I4_1/amd$). The tetragonal zircon-type is made by the infinite chains, developed along [001]. These chain units are the result of the connection along the polyhedral edges, between the eightfold coordinated *A*-site dodecahedron (AO_8 or $REEO_8$) and the TO_4 tetrahedra (Fig. 1). The AO_8 polyhedron displays two independent *A*-O atomic distances, whereas the TO_4 is an undistorted polyhedron defined by a single *T*-O bond distance. Each chain is in contact with 4 others in the (001) plane, by means of the connecting edges along a AO_8 units and the four surroundings. Due to the high symmetry space group ($I4_1/amd$) the zircon structure shows only three independent atomic coordinates.

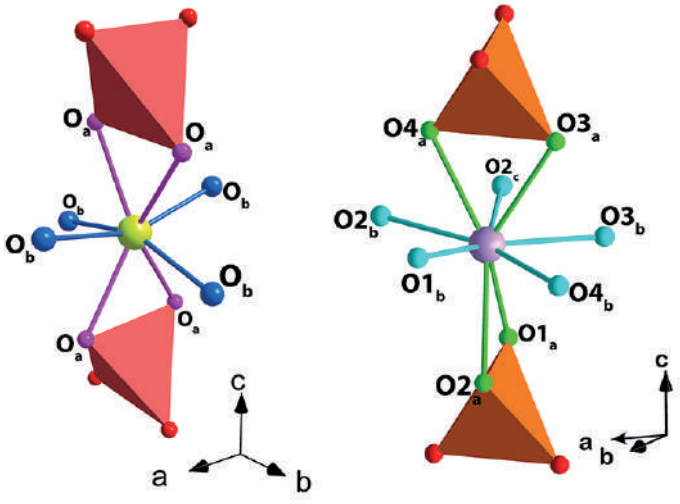

Figure 1 *Crystal structure of* ***a)*** *zircon- and* ***b)*** *monazite-type minerals, showing the architecture of the chain-unit and REE-coordination polyhedron*

The so-called monazite-type crystal structure crystallizes in the $P2_1/n$ space group. The monazite-type structure is characterized by the REE site in ninefold coordination. As the zircon-type, the monazite-type structure is characterized by infinite chains running along the [001] direction (*c*-axis), composed by the alternation of the REE-coordination polyhedra and the *T*-hosting tetrahedra (Fig. 1). The REE-polyhedron coordination environment is made by nine symmetrical independent oxygen atoms ($REEO_9$) and it can be described as an equatorial pentagon (sharing vertices with five TO_4 tetrahedra of five adjacent chains in correspondence of the $O1_b$, $O2_b$, $O2_c$, $O3_b$ and $O4_b$ oxygen atoms), interpenetrated by a tetrahedron (made by the $O1_a$, $O2_a$, $O3_a$ and $O4_a$ oxygen atoms, see Fig. 2, which is in contact, along the [001] direction, with two subsequent TO_4 tetrahedra, leading to the formation of the infinite chain units. According to the notation reported in Fig. 2, the REE-$O2_a$ bond length is sharply longer than the other REE-O bonds, contributing to a significant distortion of the $REEO_9$ polyhedron (Clavier et al. 2011).

MATERIALS AND METHODS

Fourteen rock specimens, pertaining to different Alpine quartz-bearing fissures, have been selected from the personal collection of the Italian collector Enzo Sartori, all sampled from the Mt. Cervandone area between 2000 and 2020. They were first observed under a stereomicroscope, with the aim to identify their mineralogical assemblage, which was later confirmed by single-crystal X-ray diffraction and spectroscopic analysis. Fifteen REE-bearing phosphate and arsenate crystals have been selected and extracted from the fourteen rock specimens under study (see Pagliaro et al., 2022a for the details), and then characterized by means of electron probe microanalysis in wavelength dispersion mode (EPMA-WDS), single-crystal X-ray diffraction, Raman spectroscopy and non-ambient X-ray diffraction studies.

Non-ambient characterization

In situ high-pressure single-crystal synchrotron X-ray diffraction experiments have been conducted at two different synchrotron beamlines: the P02.2 extreme condition beamline at Desy Petra III facilities (Hamburg, Germany) and the ID15b beamline at the European Synchrotron Radiation Facility, ESRF (Grenoble, France). The single crystal XRD experiments under pressure interested all the four minerals under investigation and they have been performed using a diamond anvil cell (DAC), as a device to increase the pressure applied on the samples.

The high-temperature single-crystal XRD experiments have been performed at the Institute of Mineralogy and Petrology of the University of Innsbruck. The data collection has been conducted using a Stoe IPDS II diffractometer system with a Heatstream H*T* device, which provides a continuous hot N_2 flux and the diffraction pattern has been collected using an image plate detector.

Two combined, isothermal H*P*–H*T* single-crystal X-ray diffraction ramps have been collected on both chernovite-(Y) and monazite-(Ce). Resistive heated DAC has been

used as devices to increase both temperature and pressure.

RESULTS AND DISCUSSION

Crystal chemistry characterization

Chemical composition

Thorium is the most variable element among all the points of analysis for both zircon- and monazite-type minerals. The enrichment of Th within the REETO_4 compounds is controlled by two potential substitution mechanisms:

$$(Th, U)^{4+} + Ca^{2+} = 2REE^{3+}$$

$$(Th, U)^{4+} + Si^{4+} = REE^{3+} + (P, As)^{5+}$$

respectively known as cheralite and thorite substitution mechanisms. In Fig. 2, all the data are reported in a P/(P+As+Si) *vs.* Y diagram, which clearly allows to distinguish between the four minerals under investigation, arranged in four distinct quadrants. The Y-poor side of the diagram contains the chemical data from the monazite-(Ce) and gasparite-(Ce) crystals, respectively enriched in P and As. Data from chernovite-(Y) and xenotime-(Y) lie on the Y-enriched side of the diagram and are characterized by a highly variable P and As fraction, resulting in an almost complete solid solution along the join chernovite-(Y)–xenotime-(Y). On the other side, the composition of gasparite-(Ce) and monazite-(Ce) crystals is closer to the ideal endmembers, and only a partial solution is observed.

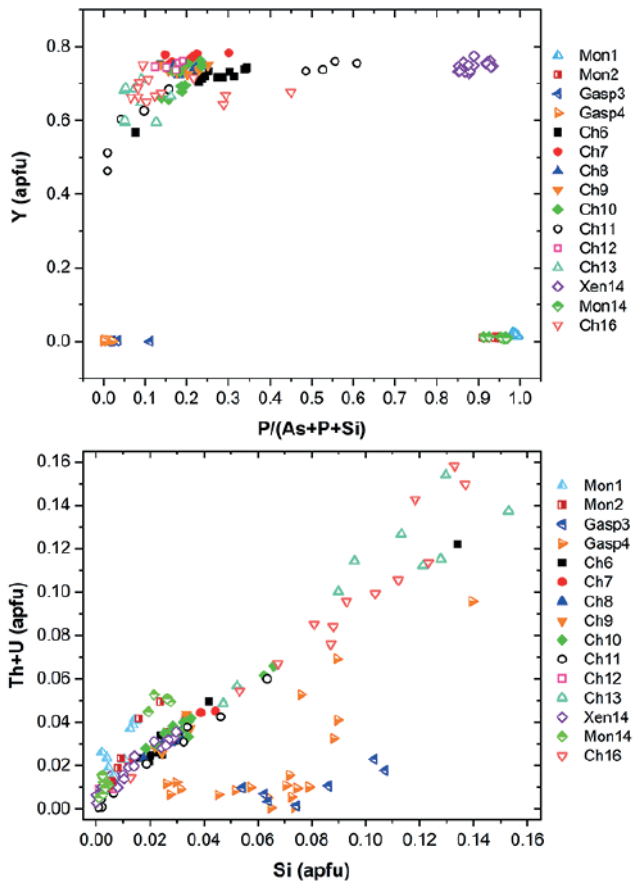

Figure 2 a) *P/(P+As+Si) vs. Y diagram and* ***b)*** *Si vs. Th+U (in apfu) for all the samples under investigation*

The *A*-site of the chernovite-(Y)–xenotime-(Y) series is characterized by a relatively constant composition, where Y is always the dominant cation (ranging from a maximum of 0.78 a.p.f.u. to a minimum of 0.46 a.p.f.u.), followed, on average, by Dy, Er, Gd, Yb and Ho. When the Y content is lower than ~0.6 a.p.f.u., Th or LREE become relevant *A*-site occupying cations.

The REE pattern for all the samples under investigation is reported in Fig. 3, normalized to the REE concentration of the Carbonaceous Chondrite C1. As mentioned above, the tetragonal structure of chernovite-(Y) and xenotime-(Y) has a strong preference for Y and, in general, the smaller HREE: this pattern is reflected by the positive slope reported in Fig. 3. Conversely, in the gasparite-(Ce)–monazite-(Ce) series, the LREE enrichment is responsible for the negative slope in Fig. 3. It is worthwhile to point out that the relatively high Gd content, shown by the three monazites under investigation, has been already described in alpine-fissures minerals related to the circulation of hydrothermal fluids, as in the case of Mt. Cervandone.

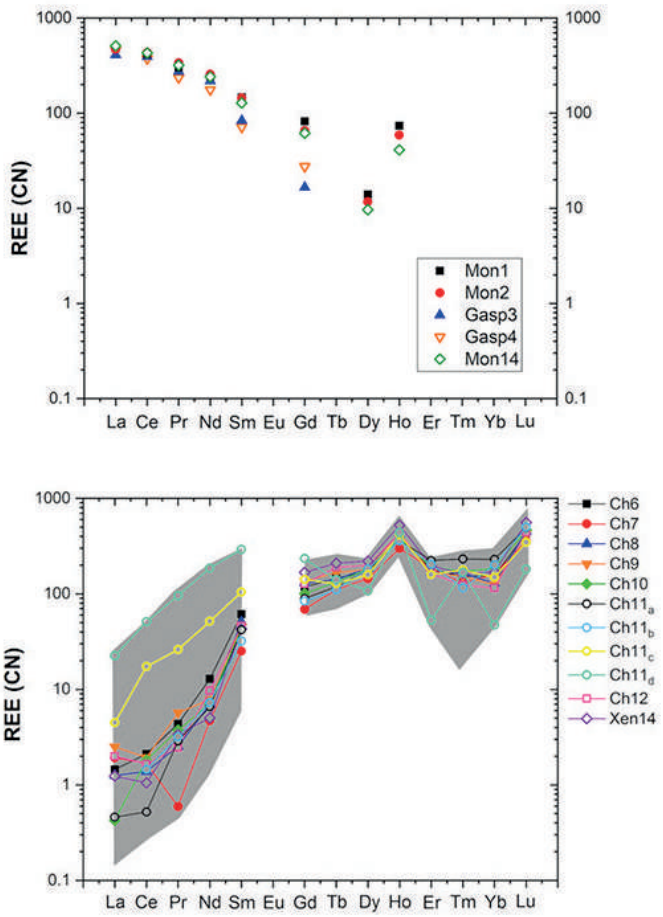

Figure 3 *Average composition of REE (normalized to the CN-1 chondrite, after Wasson and Kallemeyn (1988)) of all the samples of the gasparite-(Ce)-monazite-(Ce) series* ***a)*** *and of the chernovite-(Y)-xenotime-(Y) series* ***b)****. The grey belt in b) represents the range of the lanthanides composition for all the points of analysis of the chernovite-(Y)-xenotime-(Y) series. For sample Ch11 in b) are reported four distinct chemical compositions, due to its strong chemical zonation (see Pagliaro* et al. *2022a for further details)*

Although the trivalent cations are always dominant within the *A*-site of the tetragonal series, some data points from the samples Ch6, Ch10, Ch11, Ch13 and Ch16 show a relatively large amount of Th. The thorite substitution mechanism likely occurs in the chernovite-(Y)–xenotime-(Y) series under investigation, as suggested by the strong positive linear correlation between Si and the Th+U fraction (Fig. 2). For a better representation of the crystal-chemistry of the mineral samples of this study, the (tetragonal) 2-component system chernovite-(Y)–xenotime-(Y) could be replaced by a 3-component solid solution between the endmembers chernovite-(Y), xenotime-(Y) and $ThSiO_4$. The most Th-enriched analyses on the chernovite-(Y)-xenotime-(Y) edge belong to Ch13 and Ch16, which are also characterized by a highly altered, likely metamictict texture and variable composition. In these cases, the major chemical variations concern a strong Th-enrichment, reflected by a $ThSiO_4$ up to 15 mol%. Moreover, these samples are also characterized by a larger fraction of CaO (up to 1.93 wt%, in Ch16, *vs.* an average 0.1(3) wt% for the other chernovite-(Y) samples), suggesting the occurrence of the cheralite substitution mechanism as well.

All the gasparite-(Ce) and monazite-(Ce) samples show a rather similar composition of the ninefold-coordinated *A*-site and the main differences concern in particular the abundance of Y and Ca. A relatively high amount of Y (Y_2O_3 on average, 0.7(2) wt%) is shown by the three monazite-(Ce) samples investigated, whereas this element is almost absent in the two gasparite-(Ce) samples (Y_2O_3 < 0.13 wt%). Unlike monazite-(Ce), gasparite-(Ce) shows a higher content and more uniform distribution of Ca (CaO 1.8(2) wt%, *vs* 1.1(4) wt% for monazite-(Ce). Also, in the gasparite-(Ce)–monazite-(Ce) series, Th has been found as the most variable element and, in addition, gasparite-(Ce) incorporates the highest fraction of Si among the investigated REE minerals. In this case, a further charge-compensating mechanism should be involved, to fully explain the anomalous amount of Ca and Si, not compensated by Th+U. The presence of monovalent anions, such as OH^-, F^- or Cl^-, in place of O^{2-}, may compensate for the presence of Si and Ca, according to the following equation:

$$2(OH, F, Cl)^- + Ca^{2+} + Si^{4+} = 2O^{2-} + REE^{3+} + (P, As)^{5+}$$

According to this equation, if just OH^- is taken into account, the corresponding amount of H_2O necessary to compensate the charge defect is, on average, ~0.45 wt% for both Gasp3 and Gasp4. The occurrence of some hydroxyl is corroborated by the Raman spectra, showing some peaks in the so-called hydroxyl region (Pagliaro *et al*. 2022b).

Instead, for all the samples of monazite-(Ce), the combination of cheralite and thorite substitution fully satisfies the pattern shown in Fig. 2.

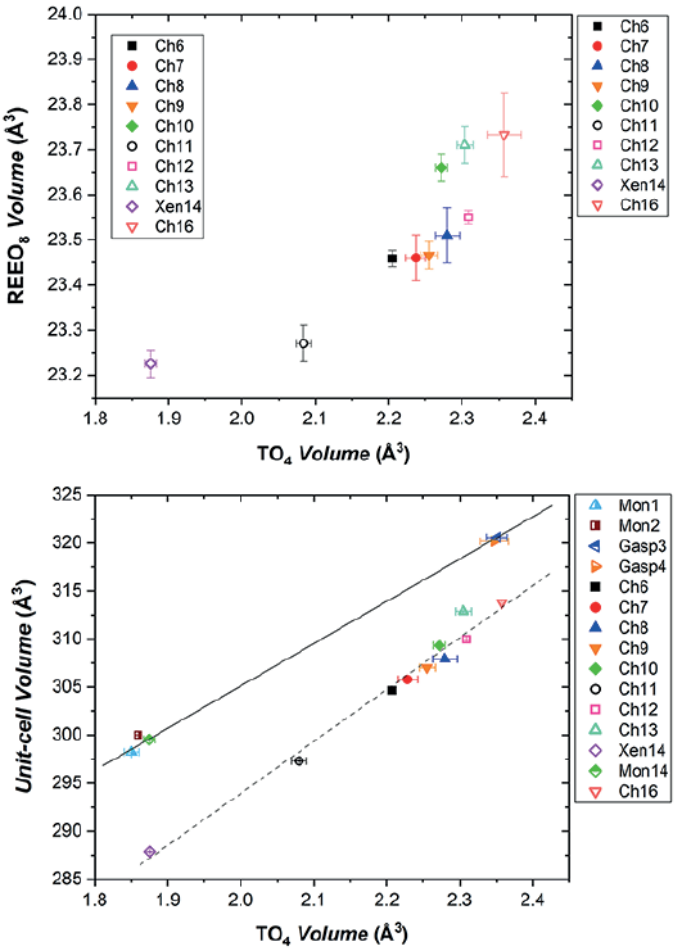

Figure 4 a) *Volume of the TO_4 tetrahedron vs. volume of the (REE)-bearing A-polyhedron for the samples pertaining to the chernovite-(Y)–xenotime-(Y) series.* ***b)*** *Volume of the TO_4 tetrahedron vs. unit-cell volume for all the samples investigated*

Crystal structural characterization

The atomic structural models refined for all the samples under study are reported in Fig. 4. It has been demonstrated that the chemical composition of the *T*-site exerts strong control over all the other structural features in zircon-type minerals. Indeed, a correlation between the P (and As) content and the unit-cell volume has been clearly determined. In addition, a correlation among the volumes of (P, As)-tetrahedra (directly related to the chemical composition of the *T*-site) and the *A*-site polyhedra is also shown by the synthetic REE*T*O_4 compounds, which structural models are reported in the International Crystal Structure Database. A comparative analysis of the structural parameters of synthetic REE-bearing phosphates has been carried out. Given the same elemental composition of the REE-bearing *A*-site, the volume of its coordination polyhedron is different in phosphates and arsenates, being always lower in phosphates, pointing out the dominant role played by the *T*O_4 structural units (V_{TO4}~2.4 Å^3 for AsO_4 and ~1.8 Å^3 for PO_4) in controlling most of the structural parameters of the REE*T*O_4 compounds. Therefore, the REE-bearing *A*-site of the zircon-type structure behaves somehow passively, while the *T*-site exerts a strong active control over the crystal structure interatomic interactions.

Similar behaviour to that described above for the (tetragonal) chernovite-(Y)-xenotime-(Y) series is also shown by the (monoclinic) gasparite-(Ce) and monazite-(Ce). However, in this case, the distribution of the chemical compositions in two clusters close to the ideal end members prevents a robust extrapolation along the whole series (Fig. 4).

High-pressure behaviour

From the *in situ* XRD data the unit cell volumes through pressure have been determined and the bulk moduli calculated for the four minerals under investigation (see Table 1). The bulk moduli have been modelled by Birch Murnaghan equations of state.

Table 1 *Refined bulk moduli, compressibilities, first derivative bulk modulus (K'=4 fixed for the BM2-EoS) and unit-cell volumes for all the ATO_4 minerals.*

Sample	$K_{P_0\text{-}T_0}$ (GPa)	β_V (GPa^{-1})	K'	V_0 ($Å^3$)
Ch10	136(2)	0.0074(1)	3.9(4)	309.96(3)
Xen14	148(4)	0.0068(2)	3.9(5)	289.5(2)
Gasp3	108.3(1.0)	0.00923(8)	4.2(2)	320.59(3)
Mon14	121(3)	0.0083(2)	-	299.3(4)

Zircon-type minerals under compression

Both chernovite-(Y) and xenotime-(Y) undergo a phase transition. In detail, chernovite-(Y) undergoes an irreversible phase transition at about 11 GPa, to a scheelite-type structure, while xenotime-(Y) undergoes a reversible zircon-to-monazite phase transition at about 17 GPa. In the case of the xenotime-(Y), for the high-pressure polymorph (hereafter xenotime-II) it was possible to refine the unit cell volume and crystal structure model through pressure. Conversely, to previous studies, the bulk modulus of xenotime-II refined in the present study is significantly lower and substantially of the same order of magnitude of that of the ambient-pressure xenotime-(Y). Such a result is in disagreement with the literature data available on the high-pressure polymorph of YPO_4, which was reported to be significantly more compressible compared to its ambient-conditions polymorph (Lacomba-Perales et al. 2010; Zhang et al. 2009). On the other hand, it is worth mentioning that the current project relies on a larger amount of experimental data and, therefore, the modelled bulk modulus obtained in this study is believed to be more accurate.

As shown in Table 1, chernovite-(Y) is more compressible compared to xenotime-(Y), without any significant difference in the *A*-site composition (since the investigated samples are the Ch10 and Xen14, see Fig. 3). In addition, as already discussed above, the chemical composition of the *T*-site exerts a strong control on the structural features of ATO_4 minerals, especially on the *A*-site polyhedral volume and bond distances, whereas the crystal chemistry of the the *A*-site apparently has a milder role. Whether the *T*-site is mostly occupied by As or P affects the size of the *A*-site polyhedron: larger when the larger As prevails in the *T*-site, smaller when the smaller P is the prevailing tetrahedral cation. Consequently, the Y-O bond distances in chernovite-(Y) are longer, compared to the same structural parameters in xenotime-(Y). The experimental data of this study suggest that the larger *A*-site of arsenates is more compressible with respect to the smaller REE-hosting polyhedron of phosphates, at a similar chemical composition in terms of Y and HREE. Therefore, the observed different compressibility among chernovite-(Y) and xenotime-(Y) can be mainly ascribed to the different chemical composition of the *T*-site cations and its influence on the overall crystal structure.

The *A*-site coordination environment absorbs most of the compression, while the *T*-site behaves as a rather rigid unit (K_{TO_4}>300 GPa). The AsO_4 tetrahedron, indeed, is more compressible than the PO_4 one and this concurs with the higher compressibility of arsenates with respect to phosphates.

Monazite-type minerals under compression

First of all, the compressional behaviour of the investigated minerals suggests that, in general, the studied monazite-type compounds are more compressible compared to the zircon-type ones. On the other side, as pointed out by Li et al. (2009), this conclusion may be biased by the role played by the ionic radius of the *A*-site. If, on one side, the bulk modulus decreases across the Ln series from the smaller Lu to the larger La for any group of compounds (*i.e.*, phosphates or arsenates), a discontinuity associated with a stiffening (*i.e.*, an increase in the bulk modulus value) occurs when the structure topology changes from the zircon- to monazite-type. Therefore, the lower bulk moduli shown by gasparite-(Ce) and monazite-(Ce), when compared to chernovite-(Y) and xenotime-(Y) respectively, can be mainly ascribed to the significant difference in the ionic radius of their *A*-sites, rather than to the structure topology.

Most of the conclusions already discussed for the zircon-type topology can be extended to the monazite-type. Indeed, the dominant role played by the chemical composition of the *T*-site over all the other structural features can explain the different compressibilities shown by monazite-(Ce) and gasparite-(Ce). Moreover, due to the low symmetry of the structure, monazite-type compounds show a strong angular deformation, which significantly concurs to the overall compression of the crystal structure. The details are discussed in Pagliaro et al. (2022b).

In addition, for both monazite-(Ce) and gasparite-(Ce) a significant change in compressional behaviour has been observed at about 18 GPa and 15 GPa, respectively. Such a behaviour has been described previously by Huang et al. (2010) and Errandonea et al. (2018), although it was considered biased by non-hydrostatic condi-

tion of the *P*-transmitting fluid during the high-pressure experiments. In the current work, a detailed structural analysis enlightened a correlation between such a change in compressional behaviour and the shortening of a "tenth" REE-O interatomic distance out from the "classical" ninefold coordinational sphere of the REE atom at ambient conditions. Therefore, such a change in compressional behaviour is likely to be influenced by a rearrangement of the crystal structure due to the increase in the coordination number of the $REEO_x$ polyhedron from nine to ten. For monazite-type compounds, such a behaviour has never been described in literature before and it could represent a link between the monazite-type structure, characterized by a ninefold coordination of the *A* atom and the post-barite-type ($P2_12_12_1$ space group, Ruiz-Fuertes et al. 2016), one of the high-pressure polymoph of monazite, which is characterized by an elevenfold *A*-site.

High-temperature behaviour

The thermal behaviour of chernovite-(Y), xenotime-(Y) and monazite-(Ce) has been modelled using a Holland-Powell equation of a state, a polynomial and a linear fits. For gasparite-(Ce), due to the small size of the crystals available, no high-temperature experiment has been carried out. The corresponding results are reported in Table 2.

Table 1 *Refined bulk moduli, compressibilities, first derivative bulk modulus (K'=4 fixed for the BM2-EoS) and unit-cell volumes for all the ATO_4 minerals.*

sample	α_V ($\times 10^{-6}$ K^{-1})	V_0 ($Å_3$)	LTEC ($\times 10^{-6}$ K^{-1})	V_0 ($Å^3$)
Ch10	9.7(1)	307.02(3)	4.81	306.74
Xen14	9.6(1.2)	288.07(4)	6.00	287.73
Mon14	19.9(1.3)	297.97(5)	9.73	297.50

In the first place, in all the cases, similar behaviour of the *A*-site polyhedron and of the *T*-site tetrahedron can be observed: in all three minerals, the thermal expansion of the REE-polyhedron is larger compared to the bulk unit-cell, while the *T*-site tetrahedron is largely less expandable. Secondly, the behaviour under heating of the monazite- and zircon-type structures is significantly different. Monazite-(Ce) is significantly more expansible compared to the zircon-type minerals studied in the present study.

It is also reasonable to state that the phosphates are more expansible than the zircon-type arsenates studied in the present work. On the other hand, the lack of the H*T* ramp on gasparite-(Ce) does not allow a complete comparison among the zircon- and monazite-type phosphates and arsenates, although Li et al. (2009) corroborate that monazite-type $REEAsO_4$ are less expansible compared to $REEPO_4$. Following the discussion carried out in the previous section, the expansive behaviour of arsenates and phosphates may be correlated *indirectly* with the role played by the TO_4 units.

The structure is affected by a chemical deformation, driven by the composition of the *T*-site atom: indeed, in the ATO_4 arsenates, the volume of the REE coordination polyhedron is larger compared to that of the isostructural phosphates. As reported by Zhang et al. (2008) and Li et al. (2009), the calculated bond distances thermal expansion of ATO_4 compounds is larger with decreasing bond length. In this light, the different behaviour of phosphates and arsenates is bound to the different *A*-O bond lengths, in turn, controlled by the chemical composition of the *T*-site, following the model previously described.

Combined high-temperature and high-pressure behaviour

Eventually, for chernovite-(Y) and monazite-(Ce), the *P-V-T* equation of state has been fitted to the H*P* (at ambient-*T*), H*T* (at ambient-*P*) and combined H*T*–H*P* data, by using a 2nd order Birch-Murnaghan EoS and a modified Holland-Powell EoS and refining a constant $(dK/dT)_P$. The corresponding refined room-*T* α_V and *K* are rather close to the thermos-elastic parameters based on individual H*P*- and H*T*-ramps of monazite-(Ce) and chernovite-(Y).

REFERENCES

Blengini, G.A., Mathieux, F., Mancini, L., Nyberg, M., & Viegas, H.M. (2020): Study on the EU's list of Critical Raw Materials. Executive Summary. Publication Office of the European Commission, Luxembourg.

Clavier, N., Podor, R., & Dacheux, N. (2011): Crystal chemistry of the monazite structure. *J. Eur. Ceram. Soc.*, **31**, 941–976.

Errandonea, D., Gomis, O., Rodríguez-Hernández, P., Muñoz, A., Ruiz-Fuertes, J., Gupta, M., Achary, S. N., Hirsch, A., Manjon, F.J., Peters, L., Roth, G., Tyagi, A.K., & Bettinelli, M. (2018): High-pressure structural and vibrational properties of monazite-type $BiPO_4$, $LaPO_4$, $CePO_4$, and $PrPO_4$. *J. Condens. Matter Phys.*, **30**, 065401.

Finch, R.J., & Hanchar, J.M. (2003): Structure and chemistry of zircon and zircon-group minerals. *Rev. Mineral. Geochem*, **53**, 1-25.

Graeser, S., & Roggiani, A.G. (1976): Occurrence and genesis of rare arsenate and phosphate minerals around Pizzo Cervandone, Italy/Switzerland. *Rendiconti della Societa Italiana di Mineralogia e Petrologia*, **32**, 279-288.

Guastoni, A., Nestola, F., Gentile, P., Zorzi, F., Alvaro, M., Lanza, A., Peruzzo, L., Schiazza, M., & Casati, N. M. (2013): Deveroite-(Ce): a new REE-oxalate from Mount Cervandone, Devero Valley, Western-Central Alps, Italy. *Mineral. Mag.*, **77**, 3019-3026.

Guastoni, A., Pezzotta, F., & Vignola, P. (2006): Characterization and genetic inferences of arsenates, sulfates and vanadates of Fe, Cu, Pb, Zn from Mt. Cervandone (Western Alps, Italy). *Period. Mineral.*, **75**, 141–150.

Huang, T., Lee, J.S., Kung, J., & Lin, C.M. (2010): Study of monazite under high pressure. *Solid State Commun.*, **150**, 1845-1850.

Lacomba-Perales, R., Errandonea, D., Meng, Y., & Bettinelli, M. (2010): High-pressure stability and compressibility of APO_4 (A= La, Nd, Eu, Gd, Er, and Y) orthophosphates: An x-ray diffraction study using synchrotron radiation. *Phys. Rev. B*, **81**, 064113.

Li, H., Zhang, S., Zhou, S., & Cao, X. (2009): Bonding characteristics, thermal expansibility, and compressibility of RXO_4 (R= Rare Earths, X= P, As) within monazite and zircon structures. *Inorg. Chem.*, **48**, 4542-4548.

Pagliaro, F., Lotti, P., Guastoni, A., Rotiroti, N., Battiston, T., & Gatta, G.D. (2022a): Crystal chemistry and miscibility of chernovite-(Y), xenotime-(Y), gasparite-(Ce) and monazite-(Ce) from Mt. Cervandone (Western Alps, Italy). *Mineral. Mag.*, **86**, 1-18.

Pagliaro, F., Lotti P., Comboni, D., Battiston, T., Guastoni, A., Fumagalli, P., Rotiroti, N., & Gatta, G.D. (2022b): High-pressure behavior of gasparite-(Ce) (nominally $CeAsO_4$), a monazite-type arsenate. *Phys. Chem. Miner.*, **49**, 1-11.

Ruiz-Fuertes, J., Hirsch, A., Friedrich, A., Winkler, B., Bayarjargal, L., Morgenroth, W., Peters, L., Roth, G., & Milman, V. (2016) High-pressure phase of $LaPO_4$ studied by x-ray diffraction and second harmonic generation. *Phys. Rev. B*, **94**, 134109.

Wasson, J.T., & Kallemeyn, G.W. (1988): Compositions of chondrites. Philosophical Transactions of the Royal Society of London. Series A, *Math. Phys. Sci.*, **325**, 535-544.

Zhang, F.X., Wang, J.W., Lang, M., Zhang, J.M., Ewing, R.C., & Boatner, L.A. (2009): High-pressure phase transitions of $ScPO_4$ and YPO_4. *Phys. Rev. B*, **80**, 18411.